On the dynamic contact angle of capillary-driven microflows in open channels

Jodie C. Tokihiro[1,†], Jean Berthier[1,†], Anika M. McManamen[1], David N. Phan[1], Sanitta Thongpang[1], Ashleigh B. Theberge[1,2]*

[1]Department of Chemistry, University of Washington, Box 351700, Seattle, Washington 98195, United States

[2]Department of Urology, University of Washington School of Medicine, Seattle, Washington 98105, United States

KEYWORDS: Young angle, dynamic contact angle, dynamic contact angle correlations, extended Lucas-Washburn law

ABSTRACT

The dynamics of a fluid flow within an open capillary channel depend on the fluid's contact angle with the channel substrate, but determining the real value of the contact angle with the solid surface is an ominous problem in capillary microflows. The Lucas-Washburn law assumes a constant contact angle during the fluid motion; however, it is observed that the contact angle of the flowing liquid with the walls differs from its static (Young) value. Correlations for the dynamic

contact angle have been proposed, and upon close inspection of Lucas-Washburn behavior in closed channels, a dynamic contact angle should be taken into account depending on the flow velocity. In this work, the dynamic contact angle in open-channel configurations is investigated using experimental data obtained with different liquids. It is shown that a dynamic contact angle must be taken into account in the early stages of the flow, i.e., at the beginning of the viscous regime when flow velocities are sufficiently high. Here, we found that amongst the different correlations for the dynamic contact angle, the Hamraoui correlation— presenting the dynamic contact angle in terms of a friction coefficient—reproduces the experimental results while other correlations overpredict the fluid velocity in open channels.

Introduction

When a fluid flows in contact with a wall, its contact angle differs from its static value — the Young contact angle. Analysis of this phenomenon dates back to the year 1979 when the first correlations between the dynamic and static contact angles were proposed.[1–3] One of these correlations is the Hoffman-Tanner's law for the spreading of a droplet on a flat substrate surface. This correlation states that the change of the contact angle during the spreading is linked to the cubic root of the capillary number — or velocity. Later, other correlations for the flow of liquids in contact with solid walls (closed channels) were proposed by Bracke *et al.*,[4] Seebergh *et al.*,[5] and Jiang *et al.,*[6] where correlations make use of the capillary number. In all of these correlations, the inertial forces are assumed to be negligible prior to the viscous forces therefore the regime is the viscous regime. More recently, Hamraoui *et al.* proposed a new correlation for viscous flows where the dynamic contact angle (DCA) is understood in terms of a friction coefficient, symbolized as β.[7]

When investigating fluid flows in capillary channels, the Lucas-Washburn (LW) law is commonly employed. However, the Lucas-Washburn law assumes a constant contact angle where close inspection of the flow velocity — for capillary rise or flow in confined channels — shows that a dynamic contact angle is present and should be taken into account (at least during the initial stage of the viscous regime when the flow velocity is high).[7–11] A detailed study of this phenomenon has been recently reported by Lunowa *et al.* for cylindrical tubes. [12]

In this work, a focus is made on the capillary flow in open channels. Contrary to traditional closed-channel microfluidics, open channels are characterized by one or more air-liquid interfaces through the removal of at least one channel wall. Open channels have recently gained traction in the microfluidics community due to advantages such as easy access to the channel contents (e.g., the ability to manipulate beads, three dimensional tissues/biospecimens) and easy fabrication or surface treatment of the microfluidic channels.[13,14] These devices are simple to operate, necessitating only a micropipette, fluid of choice, and the microfluidic device, whereas confined channels are challenging to fabricate and lack the accessibility features that open channels provide. Open microfluidics has become widely used for a variety of research fields such as cell culture, protein and metabolite assays, and organ-on-a-chip models. To some extent, the physics of the microflow in open-channel channels resembles that of confined channels, but some considerations must be adapted for open-channel flow. The LW law must be modified by using an equivalent contact angle[15] — or the so-called generalized Cassie angle — in place of the contact angle, as well as an average friction length[16] in place of the tube radius. The so-called generalized Cassie angle accounts for the air-liquid interface in an open channel — which corresponds to a contact angle of 180º — and for the different walls in the case of a composite (multi-material) channel.[15]

The average friction length scales the wall friction, and is related to the size of the channel — hydraulic diameter — and to the geometrical shape of the channel.[16]

It is shown here that, at the early stages of the viscous regime, a dynamic contact angle (DCA) best describes the fluid velocity in open channels. Based on our experiments, the most accurate correlation amongst the others is the Hamraoui correlation. The Hamraoui *et al.* correlation was developed for closed channels and zero Young contact angle. In our work, we extended the application to open channels and non-zero contact angle. Our extension is reasonable considering that the physical principles (e.g., added viscosity at the contact line) are the same. Our study employs rectangular open microfluidic channels milled in poly(methylmethacrylate) (PMMA) with slightly rounded bottom inner corners to avoid capillary filaments. In these channels, we have used different liquids such as an aqueous solution of IPA (50% v/v) (IPA 50), and solvents such as nonanol, pentanol, chloroform, FC-40 (fluorinated oil), and water.

Experimental

a. *Channel Design and Fabrication*

A channel device (Channel #1) used in the experiments is shown in Figure 1. Four different open rectangular channels milled in PMMA have been used: channel #1 (w = 1 mm, h = 2 mm), channel #2 (w = 2 mm, h = 2mm), channel #3 (w = 0.4 mm, h = 0.6 mm), and channel #4 (w = 0.4 mm, h = 0.4 mm). The characteristics of the channels are listed in Table 1. A schematic of channel #1 is shown in Figure 1. Engineering drawings of channels #1-4 can be found in Figure SI1. Figure

SIIB has two different cross-sections where the left side of the device has a cross section of w = 2 mm, h = 2 mm and the right side of the device has a cross section with the dimensions of w = 1 mm, h = 2 mm. Note that the cross section of the right side of the device shown in Figure SIIB is the same as channel #1 (Figure SIIA). Figure SIIA has a total travel distance of 306 mm and Figure SIIB has a travel distance of 122 mm for each cross section. In generating experimental data for Figures 3 and 4, the devices in Figure SIIA and SIIB were used, respectively. Calibration markers separated by a known distance apart were milled into the device for scaling purposes during image analysis (Figure 1A). The inner bottom corner of the channel is rounded during the fabrication step in order to avoid the formation of capillary filaments.[17,18] A profilometer photo of the cross-section of channel #1 with the rounded corners is shown in Figure 1B.

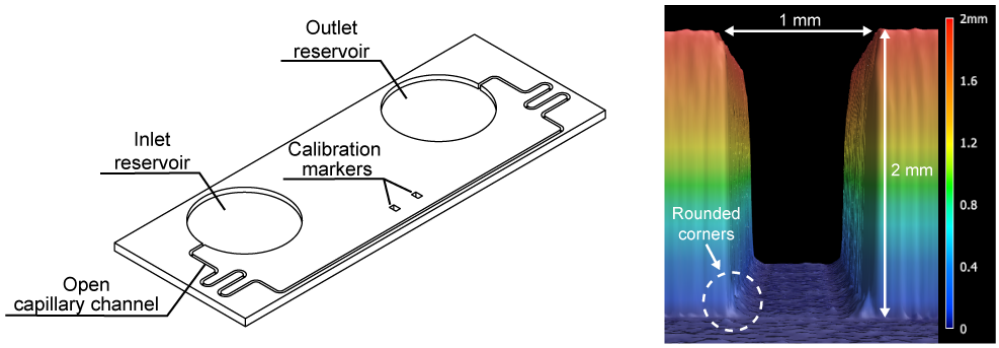

Figure 1. Isometric view of channel #1 milled in PMMA and profilometer cross-section of the channel with the rounded corners.

Table 1. Characteristics of the channels

Channel	Width	Height	Wetted perimeter	Free perimeter	Friction length

Symbol/units	*w [mm]*	*h [mm]*	p_W *[mm]*	P_F *[mm]*	$\bar{\lambda}$*[mm]*
Channel #1	1	2	5	1	0.20
Channel #2	2	2	6	2	0.40
Channel #3	0.4	0.6	1.6	0.4	0.09
Channel #4	0.4	0.4	1.2	0.4	0.07

The average friction lengths (rightmost column in Table 1) representing the wall friction are first approximated by either one of the semi-empirical formulations[19,20]:

$$\bar{\lambda} \cong \frac{1}{3}\,\frac{w+h}{\left(\frac{2h}{w}+\frac{w}{h}\right)}\,, \tag{1}$$

or

$$\bar{\lambda} \cong \frac{2}{3}\,\frac{h}{w}\,\zeta\left(\frac{h}{w}\right)(w+h), \tag{2}$$

where $\zeta\left(\frac{h}{w}\right) = 1 + 0.671\frac{h}{w} + 4.1697\left(\frac{h}{w}\right)^2$.

These two formulas produce approximate values of the friction length. These values are then adjusted on the experimental plots for the flow velocity, using velocities far from the channel

entrance, where the contact angle most resembles the static contact angle—as will be shown later in the text (Figure 2).

The channels were designed using computer aided design (CAD) software (Solidworks 2017, Waltham, MA) and the design files were converted to G-code using computer aided manufacturing (CAM) software (Fusion 360, Autodesk, San Rafael, CA). Channels were milled in poly(methyl methacrylate) (PMMA) sheets (3.175 mm thick, #8560K239; McMaster-Carr, Sante Fe Springs, CA).

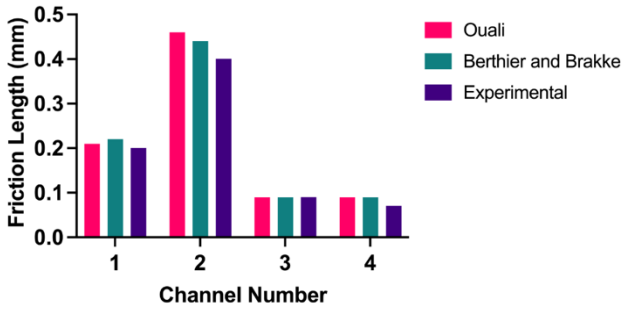

Figure 2. Comparison of the different approaches for the friction length: Ouali *et al.*[19] (pink color); Berthier and Brakke[18] (green color); experiments (purple color).

To create round bottom channels, endmills with a cutter diameter of 1/32" (TR-2-0312-BN) and 1/64" (TR-2-0150-BN) were used (Performance Micro Tool, Janesville, WI). The devices were fabricated via micro-milling on a Datron Neo computer numerical control (CNC) mill (Datron, Germany). After fabrication, the channel dimensions were confirmed using a Keyence wide-area 3D measurement VR-5000. The channel bottom is estimated to have a few microns of roughness — due to milling process — which is one magnitude below the roughness values that were observed by Lade *et al.* that would produce substantial fluctuations in velocity.[21] Note that the

effect of small roughness on open-capillary flow dynamic is not yet completely understood since small reliefs on the wall surface slightly increase the capillary force due to Wenzel effect as well as slightly increase the friction force.[22] In our case, the adjustment of the friction length indirectly takes into account this effect. Prior to device use, the devices were ultrasonicated in ethanol at a concentration of 70% (v/v) and rinsed with deionized water (DI). Devices were then allowed to dry in the fume hood overnight.

b. Solvent Preparation and Physical Properties

Different solvents have been used in this study. Aqueous solvents included: isopropyl alcohol (IPA) at a concentration of 50% (v/v) and deionized and distilled water (American Society for Testing and Materials Type II, HARLECO, Sigma-Aldrich, St. Louis, MO). These solvents were colored with 0.60 % yellow or 1.2 % blue food coloring. (McCormick). Organic compounds such as nonanol (Sigma-Aldrich, St. Louis, MO), pentanol (Sigma-Aldrich, St. Louis, MO), FC-40 (Sigma-Aldrich, St. Louis, MO), chloroform (Fisher Scientific, Hampton, NH) have been colored with either Solvent Yellow 7 or with Solvent Green 3 (Sigma-Aldrich, St. Louis, MO) at concentrations of 0.50 mg/mL and 1.43 mg/mL respectively. FC-40 was not colored, but tracking its travel in the channel was still feasible. In the case of water, the channel was previously treated by oxygen plasma no more than 30 minutes prior to experimentation, to avoid contact angle relaxation.[23]

The physical data for these liquids are listed in Table 2.

Table 2. Properties of the liquids*

	γ [mN/m]	μ [mPa.s]	θ	w [mm]	h [mm]	θ*
Water	70	1.1	46	0.4	0.6	0.30
Chloroform	28	0.6	15	1	2	0.64
IPA 50	30	3.0	18	0.4	0.4	0.46
IPA 50	30	3.0	18	1	2	0.63
IPA 50	30	3.0	18	2	2	0.46
FC-40	16	2.5	17	1	2	0.63
Pentanol	25	3.7	13	2	2	0.48
Nonanol	27	11.5	13	2	2	0.48

*Note: These values are from Mohammad *et al.* 2014[24] and Kim *et al.* 2016[25]

The values of the physical properties of the liquids have been taken from physical tables and literature[24], and the contact angles with PMMA have been measured in Kim *et al.*[25] The generalized Cassie angle, $\theta*$, is defined by:

$$cos\theta^* = \frac{p_W}{p} cos\theta_0 - \frac{p_F}{p}, \quad (3)$$

where θ_0 is the Young (static) contact angle and p_W and p_F are the wetted and free perimeters in a cross section and $p = p_W + p_F$. In the present case, assimilating the cross section to a rectangle of width, *w,* and height, *h:*

$$cos\theta^* = \frac{(w+2h)cos\theta_0 - w}{2\,(w+h)}. \quad (4)$$

a. *Open channel flow experiments*

To obtain fluid velocities, the prepared fluids were flowed through the uniform cross section channels (#1-4). In channel #1, 2.2 mL of the dyed chloroform, water, and the colorless FC-40 were added to the inlet reservoirs of individual devices. For the devices using chloroform and water, which required an extended travel distance, a refill of 300 µL of the flowing fluid was added to the inlet reservoir to minimize the effect of pressure on the fluid dynamics. A refill was not added for FC-40 since data collection stopped after the fluid front reached the first calibration marker. Data was collected for the chloroform and water experiments until the fluid front of each respective device reached the outlet reservoir. For channel #2, 2.2 mL of the dyed IPA 50, nonanol, and pentanol were added to the inlet reservoir of individual devices connected to the cross section corresponding to w = 2 mm and h = 2 mm. Data was collected until the fluid surpassed the first calibration maker. For channel #3, 140 µL of the dyed water was added to the plasma treated device and data was collected until the fluid front reached the outlet reservoir. For channel #4, 170 µL of IPA 50 was added to the inlet reservoir and data was collected until the fluid front reached the outlet reservoir. For each fluid in each channel dimension, a n = 3 was used.

Videos of the progression of the flow of the solvent in the device were recorded using a Nikon-D5300 ultra-high resolution single lens reflective (SLR) camera at 60 fps. A video frame was analyzed every 10 frames using an execution file written in Python (execution file provided in SI).

The distance that the fluid front had traveled was measured using ImageJ. The scale for each trial was set using the "Set Scale" function and the calibration markers on the device. The fluid front was tracked using the segmented line function and the total travel distance for each frame was measured using the "Measure" function. Data was exported as a .csv file and imported into Microsoft Excel. Calculations for fluid velocity and comparisons to the theoretical model were also conducted in Microsoft Excel.

Results (with Discussion)

a. Theoretical approach

The original Lucas-Washburn law for cylindrical tubes links the travel distance, *z*, to the elapsed time, *t*, by $z = \sqrt{\frac{\gamma}{\mu}\frac{R\cos\theta}{2}t}$, where γ is the surface tension between liquid and air, μ is the liquid viscosity, *R* is the cylinder interior radius, and θ is the Young contact angle. Thus, the velocity of the flow *V* depends on the travel distance by the relation

$$V = \frac{\gamma}{\mu}\frac{R\cos\theta}{4}\frac{1}{z} \tag{5}$$

Using the geometry of open-channel, the Lucas-Washburn law yields the relation between velocity, *V,* and travel distance, *z,*

$$V = \frac{\gamma}{\mu}\frac{\bar{\lambda}\cos\theta^*}{z}, \tag{6}$$

where $\bar{\lambda}$ is the average friction length which describes the wall friction, θ^* is the generalized Cassie angle which accounts for the free surface, γ is the surface tension of the liquid, and μ is the viscosity. In terms of the capillary number (Ca), relation (6) can be rewritten as:

$$Ca = \frac{\mu}{\gamma} V = \frac{\bar{\lambda} cos\theta^*}{z}. \quad (7)$$

Here, the DCA depends on the value of the velocity as represented by the capillary number. Relation (7) shows that if the travel distance is sufficient and/or if the channel cross section is sufficiently small ($\bar{\lambda}/z \ll 1$), the use of the Young contact angle is justified. Conversely, if the condition is not met, a DCA is present, which changes the dynamics of the flow.

In this section, we show that Hamraoui's correlation can be introduced in the extended LW law to take into account the dynamic contact angle. Hamraoui *et al.* have considered the case of a capillary rise in a cylindrical tube[7] and have interpreted the dynamic contact angle in terms of a molecular friction coefficient at the front of the liquid flowing over the substrate. They found the expression of the capillary force associated to this molecular effect (precursor dynamic film[7,26,27]). If θ_0 and θ correspond to the static and dynamic angle, respectively, and V is the velocity, the decrease of the capillary force (ΔF_{cap}) can be written as

$$\Delta F_{cap} = \gamma\,(cos\theta - cos\theta_0) = -\beta\, V^n, \quad (8)$$

where β and n are coefficients depending on the liquids and wall. In their theory, the value of n was found to be n=1 as the rising liquid was in contact with air. They also found that the coefficient, β, varies between 0.02 and 0.2 for ethanol mixtures and a glass capillary tube. In this case, the static value of the contact angle was $\theta_0 = 0$.

In our case, the horizontality of the channel does not preclude the general correlation (8). We can write, using the capillary number ($Ca = \mu V/\gamma$):

$$cos\theta = cos\theta_0 - \frac{\beta}{\mu}\, Ca = cos\theta_0 - \frac{\beta}{\gamma}\, V\ . \tag{9}$$

In the viscous regime, the capillary force, F_{cap}, is equal to the wall friction force, F_{drag} (whether the channel is closed or open), where

$$F_{cap} = p\,\gamma cos\theta^* = F_{drag} = p\,z\,\mu\frac{V}{\bar{\lambda}}\,. \tag{10}$$

In relation (10), z is the marching — or travel — distance, p is the total perimeter of a cross section (including the liquid/air boundary if any), $\bar{\lambda}$ is the average friction length,[16] and θ^* is the generalized Cassie angle[15]. Substituting $V = dz/dt$, relation (10) can be written as

$$zV = \frac{1}{2}\frac{dz^2}{dt} = \frac{\gamma}{\mu}\bar{\lambda}\, cos\theta^*\ , \tag{11}$$

or

$$z^2 = \frac{\gamma}{\mu}2\bar{\lambda}\int_0^t cos\theta^* dt\ , \tag{12}$$

Note that, in the case where θ^* is constant (or when the contact angle is static), the usual extended Lucas-Washburn law is retrieved. Let us recall that the generalized Cassie angle is given by:

$$cos\theta^* = \frac{p_W}{p}cos\theta - \frac{p_F}{p}. \tag{13}$$

Therefore, (12) becomes

$$z^2 = \frac{\gamma}{\mu}2\bar{\lambda}\int_0^t \left(\frac{p_W}{p}cos\theta - \frac{p_F}{p}\right) dt\ . \tag{14}$$

We can then use correlation (9) to express the dynamic contact angle

$$z^2 = \frac{\gamma}{\mu}2\bar{\lambda}\int_0^t \left[\frac{p_W}{p}\left(cos\theta_0 - \frac{\beta}{\gamma}\,V\right) - \frac{p_F}{p}\right] dt = \frac{\gamma}{\mu}2\bar{\lambda}\int_0^t \left[\left(\frac{p_W}{p}cos\theta_0 - \frac{p_F}{p}\right) - \frac{p_W}{p}\frac{\beta}{\gamma}\frac{dz}{dt}\right] dt\ , \tag{15}$$

or

$$z^2 = \frac{\gamma}{\mu} 2\bar{\lambda}\, cos\theta_0^* t - \frac{\gamma}{\mu} 2\bar{\lambda} \int_0^t \frac{p_W}{p} \frac{\beta}{\gamma} \frac{dz}{dt} dt \ . \tag{16}$$

The first term in (16) is the travel distance with the static contact angle ($z_0^2 = \frac{\gamma}{\mu} 2\bar{\lambda}\, cos\theta_0^* t$), and the second term is a correction due to the dynamic contact angle. Relation (16) can be simplified as:

$$z^2 = \frac{\gamma}{\mu} 2\bar{\lambda}\, cos\theta_0^* t - 2\bar{\lambda} \frac{p_W}{p} \frac{\beta}{\mu} z \ . \tag{17}$$

The real travel distance — accounting for the dynamic contact angle correction — is then solved using the quadratic equation:

$$z^2 + 2\bar{\lambda} \frac{p_W}{p} \frac{\beta}{\mu} z \ - z_0^2 = 0 \ . \tag{18}$$

In (18), we have to keep in mind that z and z_0 are function of the time, t. Therefore, we finally obtain:

$$z = \ -\bar{\lambda} \frac{p_W}{p} \frac{\beta}{\mu} + \sqrt{\left(\bar{\lambda} \frac{p_W}{p} \frac{\beta}{\mu}\right)^2 + z_0^2} \ . \tag{19}$$

We can verify that at t=0 (we neglect the evanescent inertial motion[28]), z_0=0 and z=0. For a long channel, z_0 becomes large and $z \rightarrow z_0$.

Flow velocity can also be easily deduced from (19) by time derivation:

$$V = \frac{V_0}{\sqrt{1+\frac{\left(\bar{\lambda}\frac{p_W}{p}\frac{\beta}{\mu}\right)^2}{z_0^2}}}\ , \tag{20}$$

where V_0 is the velocity obtained using the static contact angle, $V_0 = dz_0/dt$. When the travel distance increases, z_0 increases and the real velocity V converges towards the velocity, V_0. Note that when z_0 goes to zero, z goes to zero, and relation (20) indicates that V goes to $V(z \to 0) = V_0 z_0/\bar{\lambda}\frac{p_W}{p}\frac{\beta}{\mu} = p\,\gamma cos\theta^*/\beta p_W$, therefore showing that the coefficient, β, acts like a supplementary viscosity. However, in reality, relation (20) holds when the inertial regime ends when $z_0 > z_{inertial}$.

b. Experimental results and comparison with model

To demonstrate the need for the use of a DCA at sufficiently high fluid velocities in the laboratory setting, we have designed four open microfluidic channels of various cross sections that are uniform along the length of the channel and flowed "fast" and "slow" fluids through them. We have categorized the different liquids by their intrinsic velocity, $V_i = \gamma/\mu$. The "fast" fluids correspond to high values of V_i ($V_i \gtrsim 30\ m/s$) and "slow" fluids by low values of V_i ($V_i \lesssim 8\ m/s$). Water and chloroform are in the "fast" fluid category. Figure 3 shows the dynamics of these two fluids in channels of different cross sections. Using the method proposed in Berthier *et al.,* the travel distance vs time correlation for the Young contact angle were obtained.[16] Clearly, the LW expression using the static (Young) contact angle does not explain the flow velocity and overestimates the fluid velocity. A DCA is required to fit the experimental results as seen in Figure 3 where the experimental travel distances and velocities are closely fitted to the values predicted by the DCA theory (blue line). This DCA is obtained using β=0.35 Pa•s for water and 0.22 Pa•s

for chloroform. The β values are of the order of 0.1 to 0.2 Pa•s in the original work of Hamraoui. In our case, knowing all the other parameters (friction length, viscosity, surface tension), the values are obtained by the best fit with the experimental points.

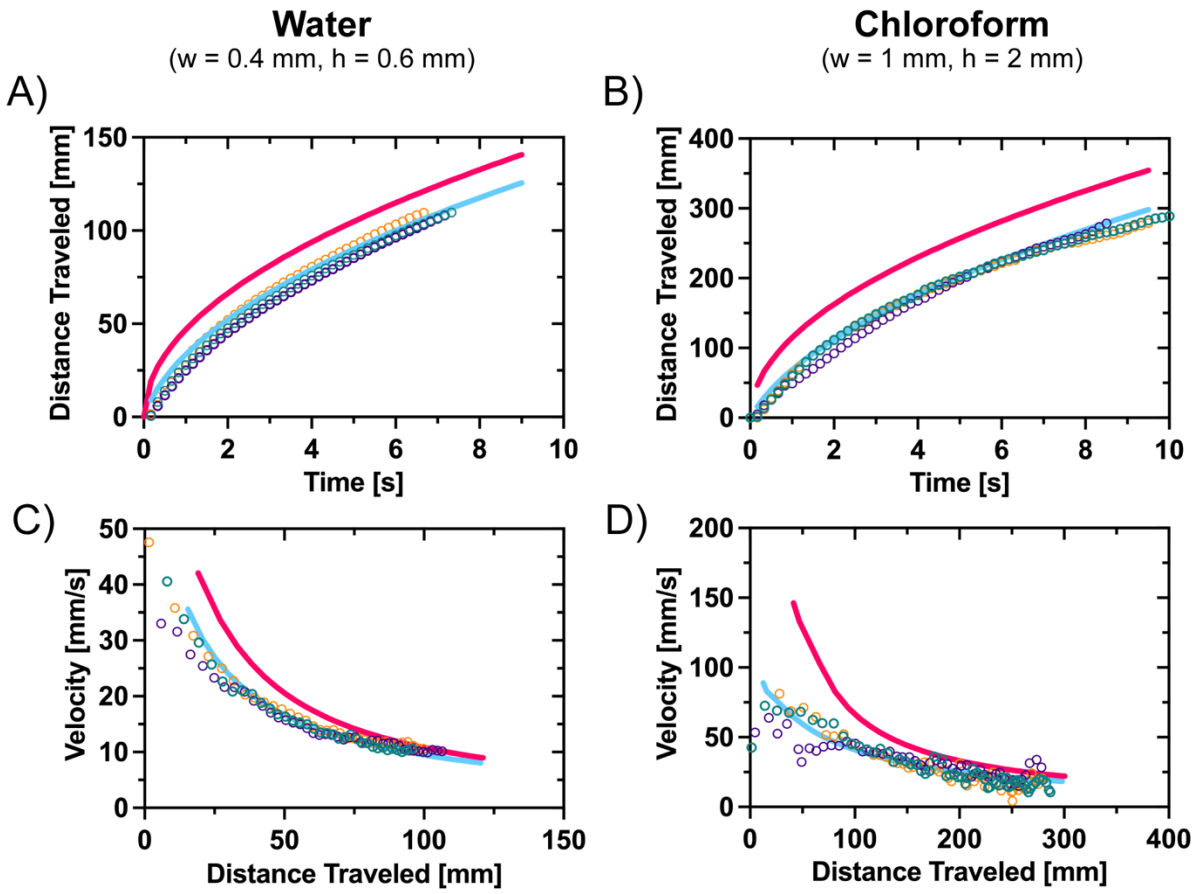

Figure 3. Experimentally determined travel distances and velocities of water and chloroform are closely fitted to the values predicted by the DCA theory. Comparison between Young (static) contact angle (pink line), DCA contact angle (blue line), and experiments (circles; three independent microfluidic devices were used for each solvent and represented in orange, green, and purple). **A:** travel distance vs. time for water in channel #3 (w = 0.4 mm, h = 0.6 mm). **B:** velocity vs. travel distance for water in channel #3. **C:** travel distance vs. time for chloroform in channel #1 (w = 1 mm; h = 2 mm); **D:** velocity vs. travel distance for chloroform in channel #1.

To demonstrate an intermediary flowing fluid, we have use a 50% (v/v) solution of IPA, which is categorized by a moderate $V_i = \gamma/\mu$ value of 10 m/s [insert the value for IPA50] which falls between 8 m/s ("slow" fluids) and 30 m/s ("fast" fluids). Figure 4 shows the dynamics of the flow in relatively large channels (w = 1 mm, h = 2 mm) (Figure 4A and B) compared to smaller cross sections (w = 0.4 mm, h = 0.4 mm) (Figure 4C and D) with the same fluid, IPA 50. In smaller cross-sections, the effect of friction at the walls is higher, resulting in a lower velocity that in larger cross-section channels, where friction has a decreased effect. In the first case, a DCA is needed to account for the dynamics as shown through the experimental data clustering around the theoretical DCA travel distances and velocities (Figure 4A and B). On the other hand, the static angle (pink line) is sufficient in the second case of small cross sections. The explanation is related to the value of the velocities, which are high in the first case, and small in the second case.

Now, in the final case of "slow" fluids, the preceding observation is still valid. Figure 5 shows a comparison of the dynamics of pentanol and nonanol in large channels (w = 2 mm, h = 2 mm) for which the wall friction is minimal. A DCA is needed in the case of pentanol (V_i~7 m/s) (Figure 5A and B), it is not the case for nonanol (V_i~2.5 m/s) (Figure 5C and D).

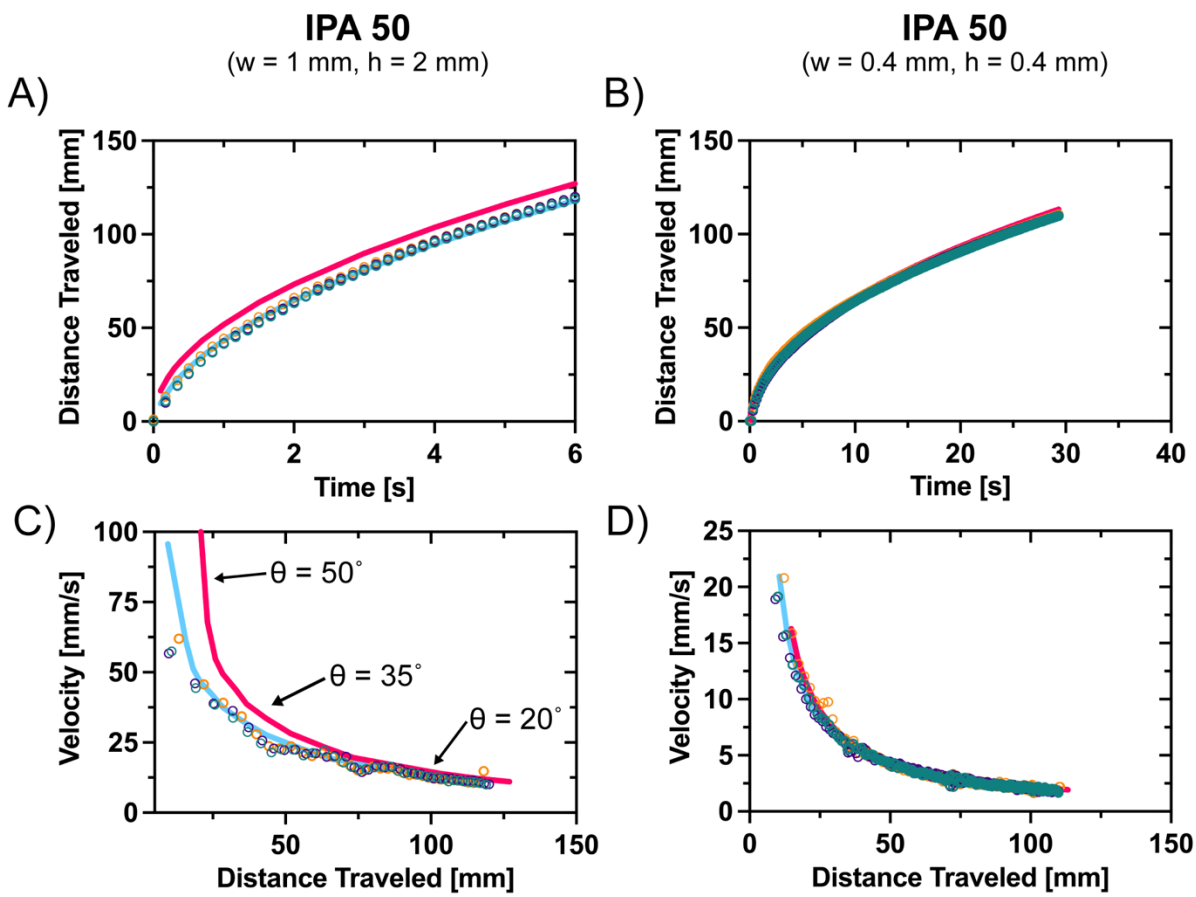

Figure 4. Experimentally determined travel distances and velocities of IPA 50 in different cross-sections are closely fitted to the values predicted by the DCA theory. Comparison between Young (static) contact angle (pink line), DCA contact angle (blue line), and experiments (circles; three independent microfluidic devices were used for each solvent and represented in orange, green, and purple). **A:** travel distance vs. time for IPA 50 in channel #1 (w = 1 mm, h = 2 mm); **B:** velocity vs. travel distance for IPA 50 in channel #1. **C:** travel distance vs. time for IPA 50 in channel #4 (w = 0.4 mm; h = 0.4 mm); **D:** velocity vs. travel distance for IPA 50 in channel #4.

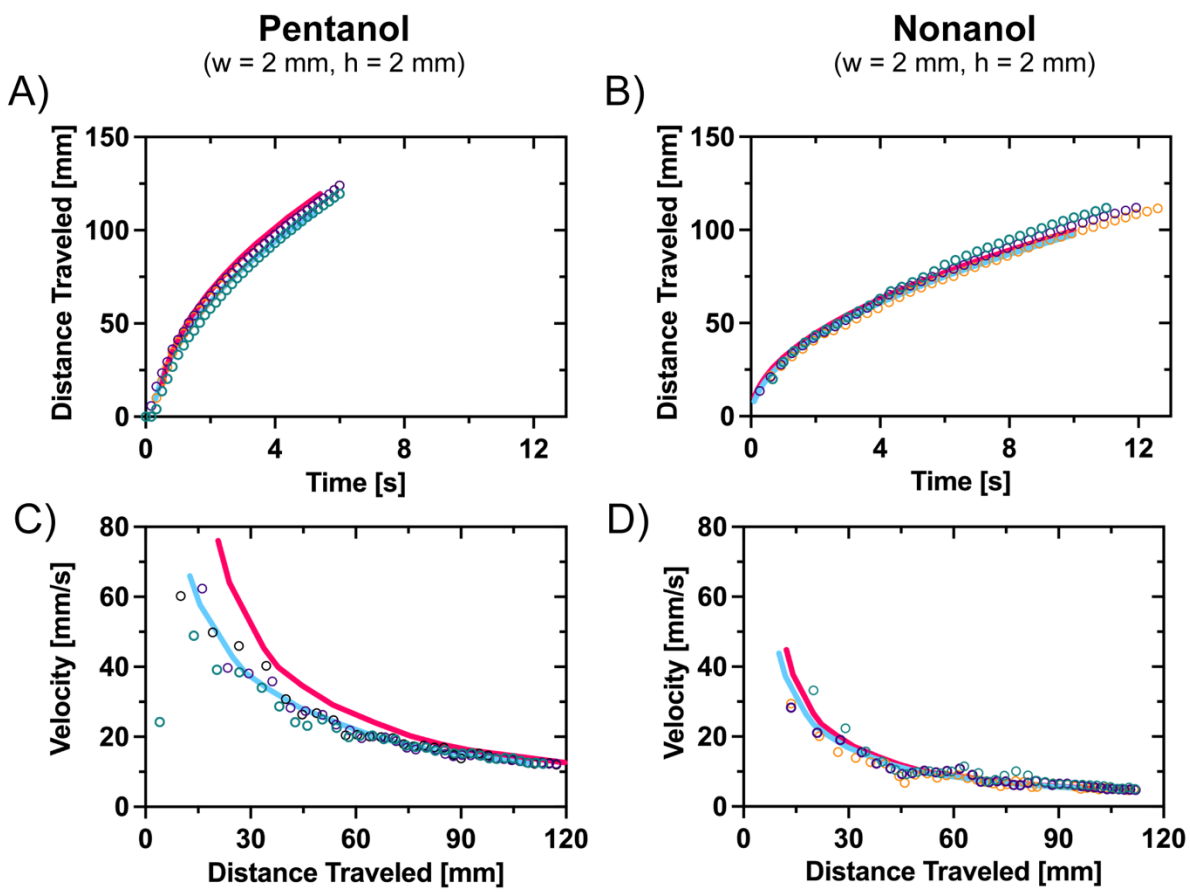

Figure 5. Experimentally determined travel distances and velocities of pentanol and nonanol are closely fitted to the values predicted by the DCA theory. Comparison between Young (static) contact angle (pink line), DCA contact angle (blue line), and experiments (circles; three independent microfluidic devices were used for each solvent and represented in orange, green, and purple). **A:** travel distance vs. time for pentanol in channel #2 (w = 2 mm, h = 2 mm); **B:** velocity vs. travel distance for pentanol in channel #2. **C:** travel distance vs. time for nonanol in channel #2 (w = 2 mm; h = 2 mm); **D:** velocity vs. travel distance for nonanol in channel #2.

c. Comparison with other correlations

In this section, we briefly present other correlations for DCA and compare them to the Hamraoui correlation used in the "*Experimental results and comparison with model*" section. These models

incorporate a capillary number in the dynamic contact angle calculation, while the Hamraoui correlation uses a friction coefficient, β,to obtain a dynamic contact angle.

The Hoffman and Tanner[1] correlation was derived for droplet spreading on a flat surface. It has been widely checked in the literature, for example by de Ruijter *et al.*[29] The correlation is

$$\theta \cong 4.5 \ Ca^{\frac{1}{3}} . \tag{21}$$

The Bracke *et al.* correlation[4] links the cosine of the dynamic contact angle to the capillary number in a closed channel:

$$cos\theta = cos\theta_0 - 2(1 + cos\theta_0)\, Ca. \tag{22}$$

This correlation is very similar to the Seebergh and Berg[5] correlation, while the Jiang *et al.* correlation[6] yields (which investigated closed channels)

$$cos\theta = cos\theta_0 - (1 + cos\theta_0)\, 4.96 \tanh\,(Ca^{0.702}) . \tag{23}$$

A numerical scheme is set up to incorporate these correlations in the LW law (Matlab[30] files included in SI). A comparison of the different correlations is shown in Figure 6. Figure 6A plots the generalized Cassie angles obtained using the different correlations for the contact angles with

the wall (Bracke, Jiang, Hoffman, Hamraoui) as a function of the capillary number. The results are very similar except for Hamraoui's correlation with a coefficient β = 0.35 Pa•s. When these correlations are used to account for the dynamics of water flow in a channel of cross section, w = 0.4 mm and h = 0.6 mm, only the Hamaroui's correlation (β = 0.35 Pa•s) produces DCA values that fits the flow dynamics (Figure 6B).

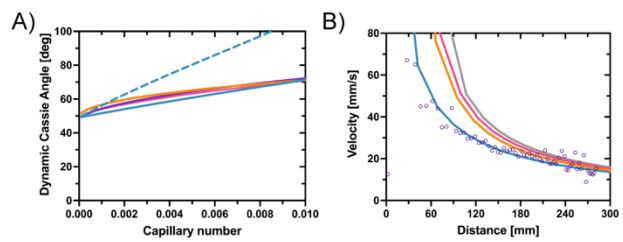

Figure 6. A: Comparison between the generalized Cassie angles obtained using the different correlations described in the text as a function of the capillary number. The two blue lines correspond to Hamraoui's[7] correlations for β = 0.12 (blue line) and 0.35 Pa•s (blue dotted line). The other correlations are: Bracke[4] (orange line), Hoffman-Tanner[1,6] (purple line), and Jiang[6] (pink line). **B:** Comparison of the velocity of a water flow in the channel #3 between experiments (circles), and different correlations: static contact angle in Lucas-Washburn law (gray line), Hamraoui DCA (blue line), Bracke DCA (orange line), and Jiang DCA (pink line).

d. Summary

In summary, "fast" flowing liquids characterized by a high intrinsic velocity ($V_{int} = \gamma/\mu$) require the use of a dynamic contact angle to describe their fluid dynamics. In the case of "slowly" flowing liquids, in moderate or small cross section open-channels, the Young (static) angle produces an adequate value of the flow velocity.

The velocity difference between DCA and static contact angle is mostly seen in the early stages of the viscous regime. At long distances, DCA and static models correspond to the same asymptotic value. Figure 7 shows the evolution of the contact angle with the distance in the channel for the different liquids of this study. The difference between "fast" and "slow" liquids clearly appears.

Notably, only the Hamraoui correlation that uses a friction coefficient produces results corresponding to the experiments. The other correlations found in the literature, even if they are valid for closed channels, do not fit the open-channel configuration.

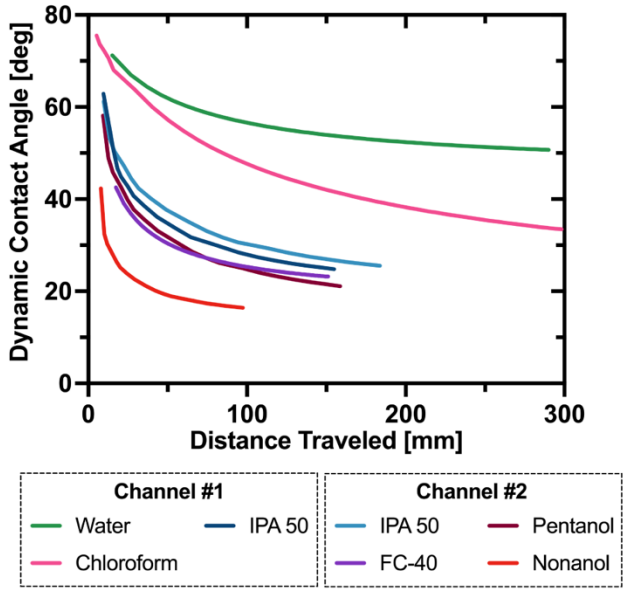

Figure 7. Evolution of the DCA over the distance in the channel for various solvents in channel(s) #1 and/or #2. Using channel #1: water (green line), chloroform (pink line), and IPA 50 (dark blue). Using channel #2: IPA 50 (sky blue line), FC-40 (lavender line), pentanol (maroon line), and nonanol (orange line).

Using (9), the DCA can be written as

$$cos\theta = cos\theta_0 - \frac{\beta}{\mu}\frac{\bar{\lambda}\, cos\theta_0^*}{z} = cos\theta_0 - \frac{\beta}{\gamma}\, V. \tag{24}$$

Although there is no theoretical background for it at this time, the experimental results suggest that the coefficient, β, depends on the intrinsic velocity as $\beta \sim (\gamma/\mu)^{0.38}$ as shown in Figure 8.

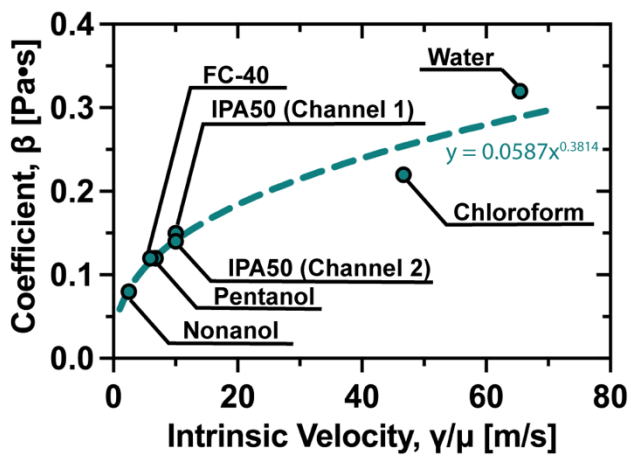

Figure 8. Experimental values of the coefficient, β, as a function of the intrinsic velocity, γ/μ.

Conclusion

In this study, a model for the dynamic contact angle of open capillary flow in the viscous regime has been developed and checked against experiments. The closed-form solution of the model shows that the real travel distance — using the dynamic contact angle — is equal to the travel distance obtained with the generalized Lucas-Washburn law for open-channels minus a correction that correlates the contact angle to the velocity. We have determined that the importance of the correction depends on the velocity of the flow. At sufficiently high velocities or long travel distances, a DCA correction is needed. In the velocity plots of every fluid presented here, we have

found that the both the DCA and Lucas-Washburn theories merge at long travel distances. Whereas in small channel cross sections or at slower velocities, the Young contact angle suffices. It is shown that Hamraoui's correlation where the dynamic contact angle is understood in terms of a friction coefficient produces accurate results while other correlations for the dynamic contact angle — Tanner *et al.*, Bracke *et al.* and Seebergh *et al.* — do not produce accurate results. The coefficient, β, appearing in the Hamraoui correlation has been fitted to the data, but needs more investigations in order to determine the strongest fit, and will be the focus of future work.

Notes

The authors declare the following competing financial interest(s): The authors acknowledge the following potential conflicts of interest in companies pursuing open microfluidic technologies however these technologies are not related to the work in this manuscript: A.B.T: Stacks to the Future, LLC.

Acknowledgements

This work was funded by NIH grant R35GM128648 (A.B.T.) and the University of Washington. We also acknowledge the M.J. Murdock Diagnostics Foundry for Translational Research. We also thank Ting Wang for assistance with figure presentation.

ASSOCIATED CONTENT

Supporting Information.

The following files are available free of charge:

Engineering drawings and comparisons with other correlations (.PDF)

Design files for channels #1-4, MATLAB codes (chloroform, IPA 50, pentanol, water), video of flow experiment of IPA 50 in Channel #4, video processing file for frame extraction (.zip)

AUTHOR INFORMATION

Corresponding Author

*Ashleigh B. Theberge (abt1@uw.edu)

Author Contributions

J.C.T., J.B., and A.M.M. designed the experiments. J.C.T., A.M.M., and D.N.P. conducted the experiments. D.N.P. wrote the Python code to extract the images from the video files. J.C.T., J.B., and A.M.M. analyzed the results. J.C.T., J.B., A.M.M., S.T., and A.B.T. interpreted the results. J.B. developed the model. J.C.T, J.B., and A.B.T. wrote the manuscript and all authors revised and approved it. †J.C.T. and J.B. contributed equally.

REFERENCES

(1) Tanner, L.H. The Spreading of Silicone Oil Drops on Horizontal Surfaces. 1979 *J. Phys. D: Appl. Phys.* **1979**, 12, 1473.

(2) Dussan, E. B. On the spreading of liquids on solid surfaces: static and dynamic contact lines. *Annu Rev Fluid Mech* **1979**, *11*, 371–400.

(3) Burley, R.; Kennedy, B. S. An experimental study of air entrainment at a solid/liquid/gas interface. *Chem Eng Sci* **1976**, *31*, 901–911.

(4) Bracke, M.; Voeght, F.; Joos, P. The Kinetics of Wetting: The Dynamic Contact Angle. *Trends in Colloid and Interface Science III* **2007**, *149*, 142–149. https://doi.org/10.1007/bfb0116200.

(5) Seebergh, J. E.; Berg, J. C. Dynamic Wetting in the Low Capillary Number Regime. *Chem Eng Sci* **1992**, *47* (17–18), 4455–4464. https://doi.org/10.1016/0009-2509(92)85123-S.

(6) Jiang, T. S.; Soo-Gun, O. H.; Slattery, J. C. Correlation for Dynamic Contact Angle. *J Colloid Interface Sci* **1979**, *69* (1), 74–77. https://doi.org/10.1016/0021-9797(79)90081-X.

(7) Hamraoui, A.; Thuresson, K.; Nylander, T.; Yaminsky, V. Can a Dynamic Contact Angle Be Understood in Terms of a Friction Coefficient? *J Colloid Interface Sci* **2000**, *226* (2), 199–204. https://doi.org/10.1006/jcis.2000.6830.

(8) Hamblin, M. N.; Hawkins, A. R.; Murray, D.; Maynes, D.; Lee, M. L.; Woolley, A. T.; Tolley, H. D. Capillary Flow in Sacrificially Etched Nanochannels. *Biomicrofluidics* **2011**, *5* (2). https://doi.org/10.1063/1.3602858.

(9) Chebbi, R. Dynamics of Liquid Penetration into Capillary Tubes. *J Colloid Interface Sci* **2007**, *315* (1), 255–260. https://doi.org/10.1016/J.JCIS.2007.06.073.

(10) Zhu, Y.; Petkovic-Duran, K. Capillary Flow in Microchannels. *Microfluid Nanofluidics* **2010**, *8* (2), 275–282. https://doi.org/10.1007/s10404-009-0516-4.

(11) Kim, H.; Lim, J. H.; Lee, K.; Choi, S. Q. Direct Measurement of Contact Angle Change in Capillary Rise. *Langmuir* **2020**, *36* (48), 14597–14606. https://doi.org/10.1021/acs.langmuir.0c02372.

(12) Lunowa, S. B.; Mascini, A.; Bringedal, C.; Bultreys, T.; Cnudde, V.; Pop, I. S. Dynamic Effects during the Capillary Rise of Fluids in Cylindrical Tubes. *Langmuir* **2022**, *38* (5), 1680–1688. https://doi.org/10.1021/acs.langmuir.1c02680.

(13) Berthier, E.; Dostie, A. M.; Lee, U. N.; Berthier, J.; Theberge, A. B. Open Microfluidic Capillary Systems. **2019**. https://doi.org/10.1021/acs.analchem.9b01429.

(14) Oliveira, N. M.; Vilabril, S.; Oliveira, M. B.; Reis, R. L.; Mano, J. F. Recent Advances on Open Fluidic Systems for Biomedical Applications: A Review. *Materials Science and Engineering: C* **2019**, *97*, 851–863. https://doi.org/10.1016/J.MSEC.2018.12.040.

(15) Berthier, J.; Brakke, K. A.; Berthier, E. A General Condition for Spontaneous Capillary Flow in Uniform Cross-Section Microchannels. *Microfluid Nanofluidics* **2014**, *16* (4), 779–785. https://doi.org/10.1007/s10404-013-1270-1.

(16) Berthier, J.; Gosselin, D.; Berthier, E. A Generalization of the Lucas–Washburn–Rideal Law to Composite Microchannels of Arbitrary Cross Section. *Microfluid Nanofluidics* **2015**, *19* (3), 497–507. https://doi.org/10.1007/s10404-014-1519-3.

(17) Concus, P.; Finn, R. ON THE BEHAVIOR OF A CAPILLARY SURFACE IN A WEDGE. *Proceedings of the National Academy of Sciences* **1969**, *63* (2), 292–299. https://doi.org/10.1073/pnas.63.2.292.

(18) Berthier, J.; Brakke, K. A.; Gosselin, D.; Huet, M.; Berthier, E. Metastable Capillary Filaments in Rectangular Cross-Section Open Microchannels. *AIMS Biophys* **2014**, *1* (1), 31–48. https://doi.org/10.3934/biophy.2014.1.31.

(19) Ouali, F. F.; McHale, G.; Javed, H.; Trabi, C.; Shirtcliffe, N. J.; Newton, M. I. Wetting Considerations in Capillary Rise and Imbibition in Closed Square Tubes and Open Rectangular Cross-Section Channels. *Microfluid Nanofluidics* **2013**, *15* (3), 309–326. https://doi.org/10.1007/s10404-013-1145-5.

(20) Lee, J. J.; Berthier, J.; Theberge, A. B.; Berthier, E. Capillary Flow in Open Microgrooves: Bifurcations and Networks. *Langmuir* **2019**, *35* (32), 10667–10675. https://doi.org/10.1021/acs.langmuir.9b01456.

(21) Lade, R. K.; Hippchen, E. J.; Macosko, C. W.; Francis, L. F. Dynamics of Capillary-Driven Flow in 3D Printed Open Microchannels. *Langmuir* **2017**, *33* (12), 2949–2964. https://doi.org/10.1021/acs.langmuir.6b04506.

(22) Bamorovat Abadi, G.; Bahrami, M. The Effect of Surface Roughness on Capillary Rise in Micro-Grooves. *Sci Rep* **2022**, *12* (1), 14867. https://doi.org/10.1038/s41598-022-19111-w.

(23) Vesel, A.; Mozetic, M. Surface Modification and Ageing of PMMA Polymer by Oxygen Plasma Treatment. *Vacuum* **2012**, *86*, 634–637.

(24) Mohammad, A. A.; Alkhaldi, K. H. A. E.; Altuwaim, M. S.; Al-Jimaz, A. S. Effect of Temperature and Chain Length on the Viscosity and Surface Tension of Binary Systems of N,N-Dimethylformamide with 1-Octanol, 1-Nonanol and 1-Decanol. *Journal of Chemical Thermodynamics* **2014**, *74*, 7–15. https://doi.org/10.1016/j.jct.2014.03.022.

(25) Kim, S.; Thiessen, P. A.; Bolton, E. E.; Chen, J.; Fu, G.; Gindulyte, A.; Han, L.; He, J.; He, S.; Shoemaker, B. A.; Wang, J.; Yu, B.; Zhang, J.; Bryant, S. H. PubChem Substance and Compound Databases. *Nucleic Acids Res* **2016**, *44* (Database issue), D1202. https://doi.org/10.1093/NAR/GKV951.

(26) Popescu, M. N.; Oshanin, G.; Dietrich, S.; Cazabat, A. M. Precursor Films in Wetting Phenomena. *J Phys Condens Matter* **2012**, *24* (24). https://doi.org/10.1088/0953-8984/24/24/243102.

(27) De Gennes, P. G. Wetting: Statics and Dynamics. **1985**.

(28) Quéré, D. Inertial Capillarity. *Europhys Lett* **1997**, *39* (5), 533–538. https://doi.org/10.1209/epl/i1997-00389-2.

(29) De Ruijter, M.J. ; Charlot, M. ; Voué, M.; De Coninck, J. Experimental Evidence of Several Time Scales in Drop Spreading, *Langmuir* **2000**, 16, 2363-2368

(30) MATLAB. ttps://fr.mathworks.com/

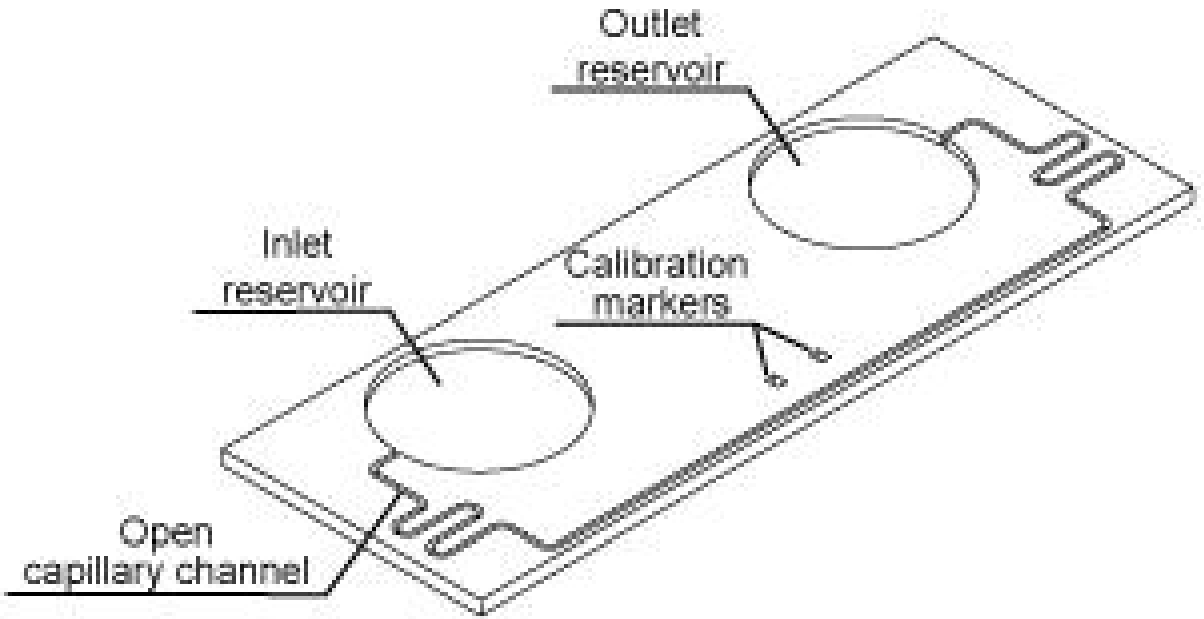
Outlet
reservoir
Inlet
reservoir
Calibration
markers
Open
capillary channel

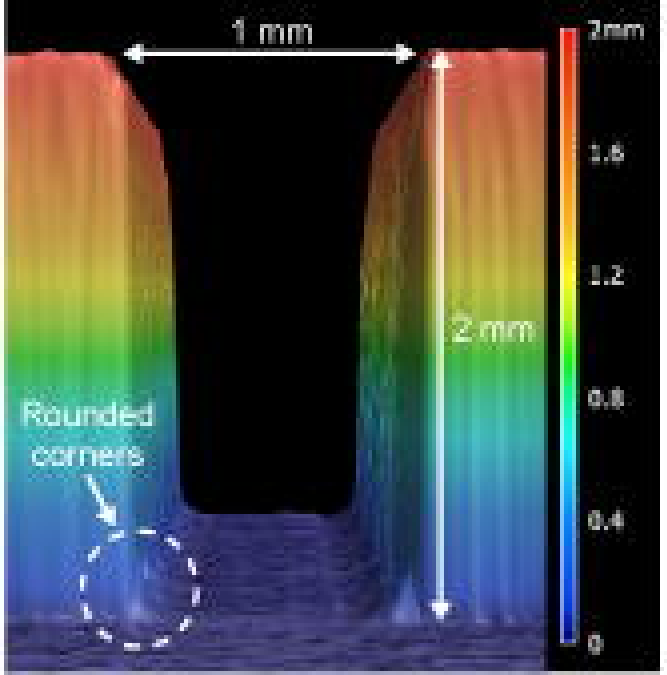
1 mm
2 mm
Rounded
corners
2mm
1.6
1.2
0.8
0.4
0

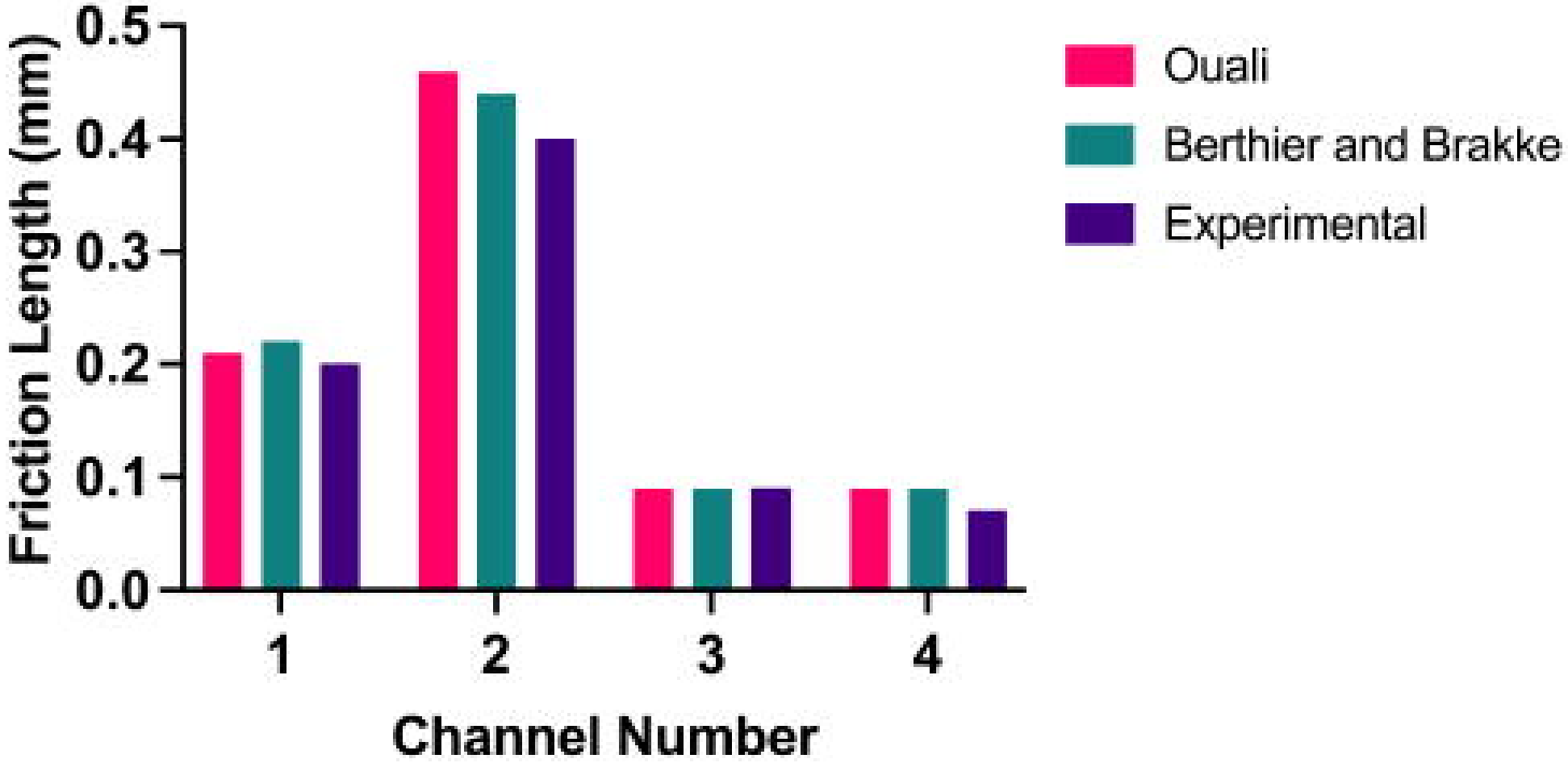
Friction Length (mm)
0.0
0.1
0.2
0.3
0.4
0.5
1
2
3
4
Channel Number
Ouali
Berthier and Brakke
Experimental

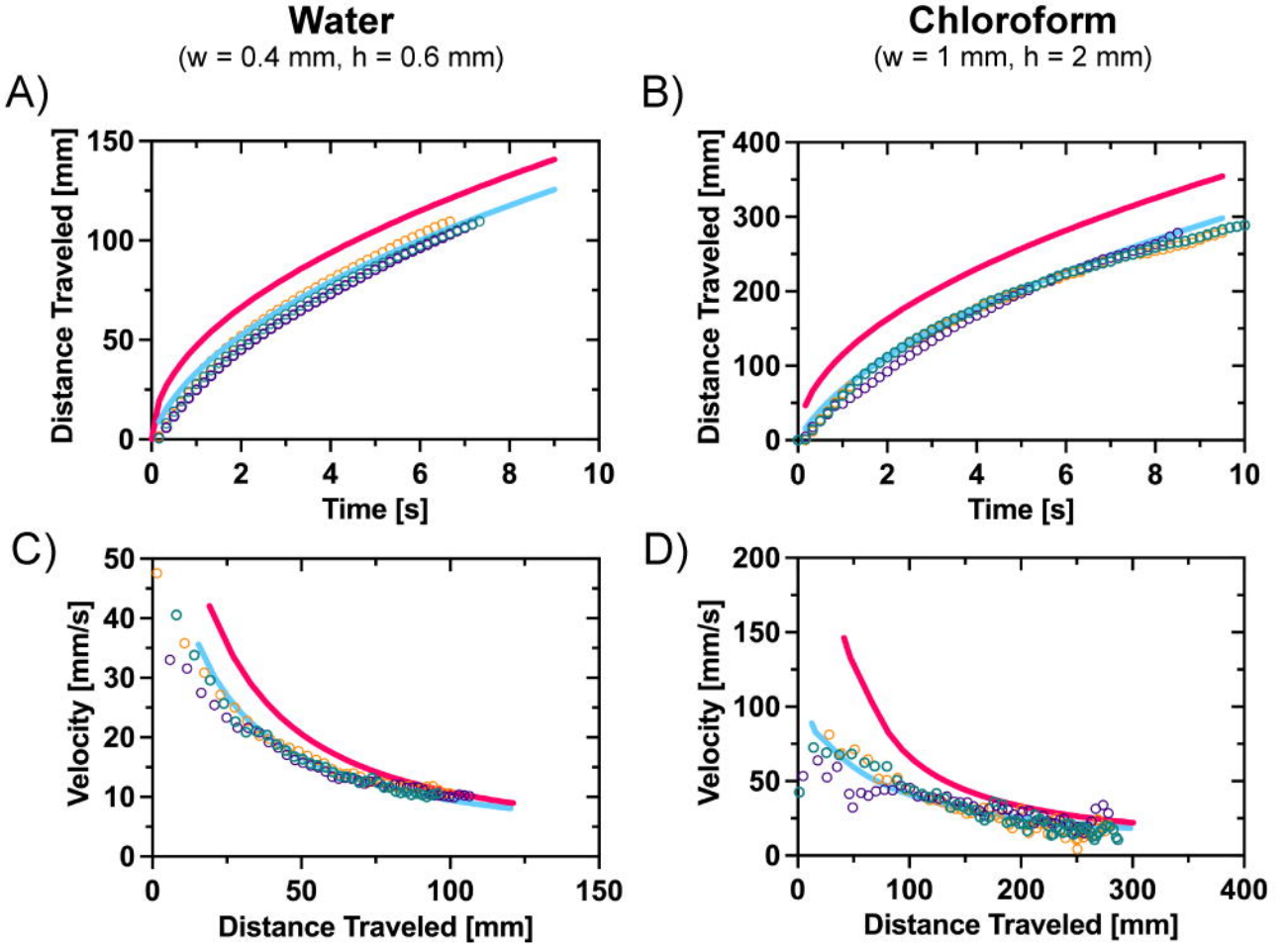
Water
(w = 0.4 mm, h = 0.6 mm)
Chloroform
(w = 1 mm, h = 2 mm)
A)
B)
C)
D)
Distance Traveled [mm]
Time [s]
Velocity [mm/s]
Distance Traveled [mm]

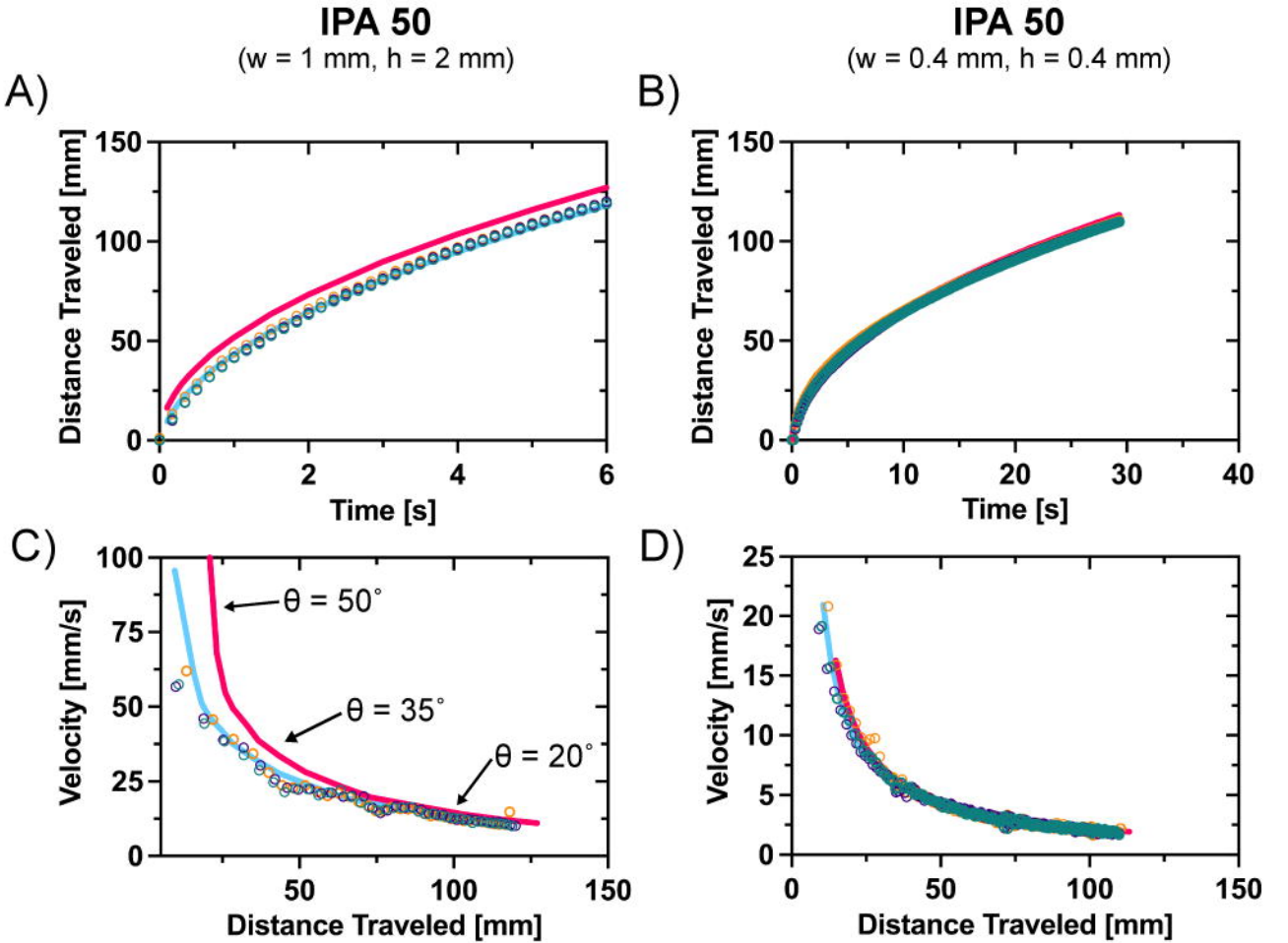
IPA 50
(w = 1 mm, h = 2 mm)
IPA 50
(w = 0.4 mm, h = 0.4 mm)
A)
B)
C)
D)
Distance Traveled [mm]
Time [s]
Velocity [mm/s]
θ = 50°
θ = 35°
θ = 20°

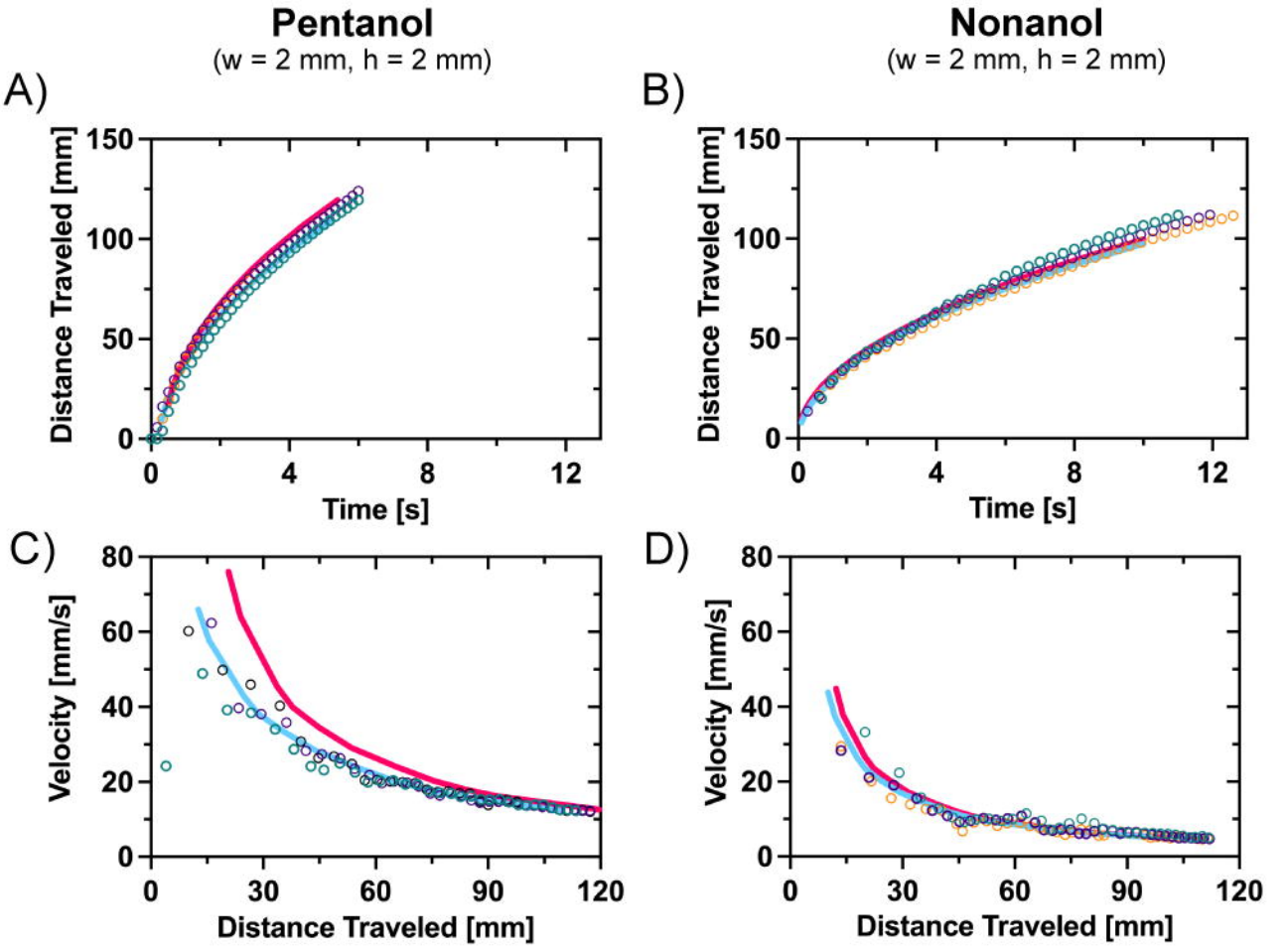
Pentanol
(w = 2 mm, h = 2 mm)
Nonanol
(w = 2 mm, h = 2 mm)
A)
B)
C)
D)
Distance Traveled [mm]
Time [s]
Velocity [mm/s]
Distance Traveled [mm]
0
50
100
150
0
4
8
12
0
20
40
60
80
0
30
60
90
120

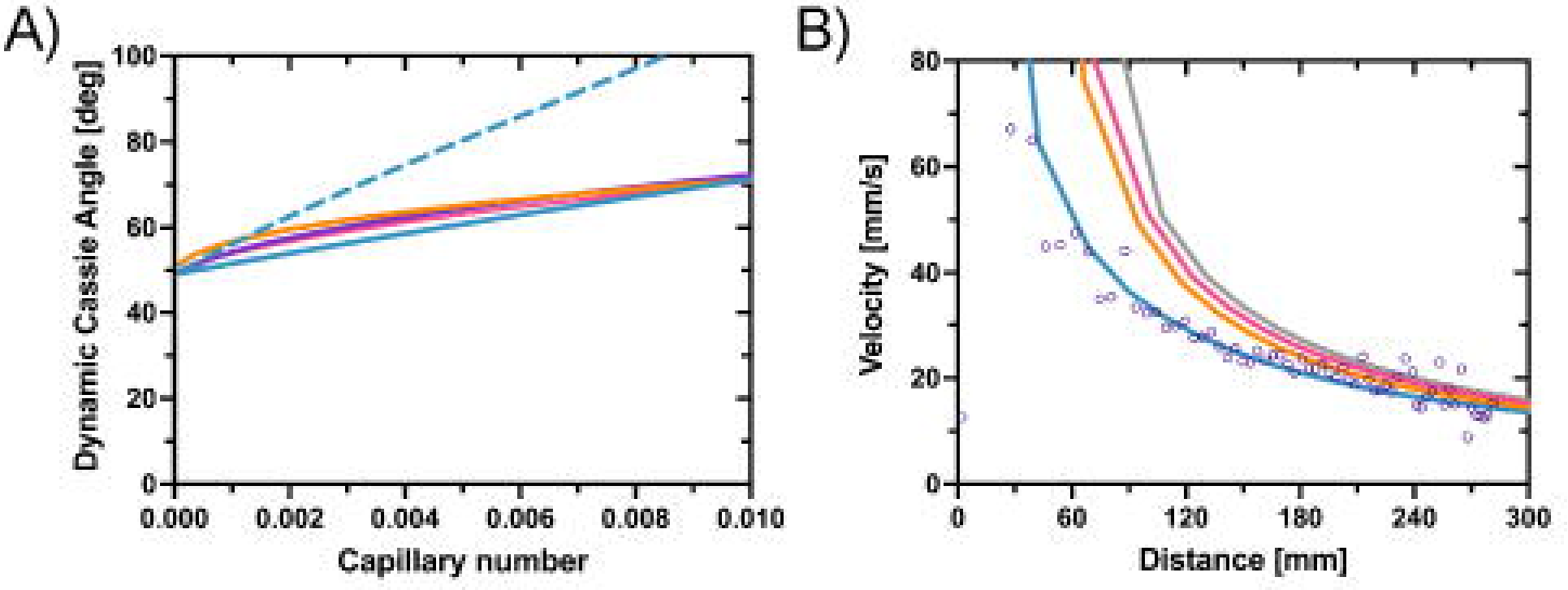
A)
Dynamic Cassie Angle [deg]
0
20
40
60
80
100
0.000
0.002
0.004
0.006
0.008
0.010
Capillary number
B)
Velocity [mm/s]
0
20
40
60
80
0
60
120
180
240
300
Distance [mm]

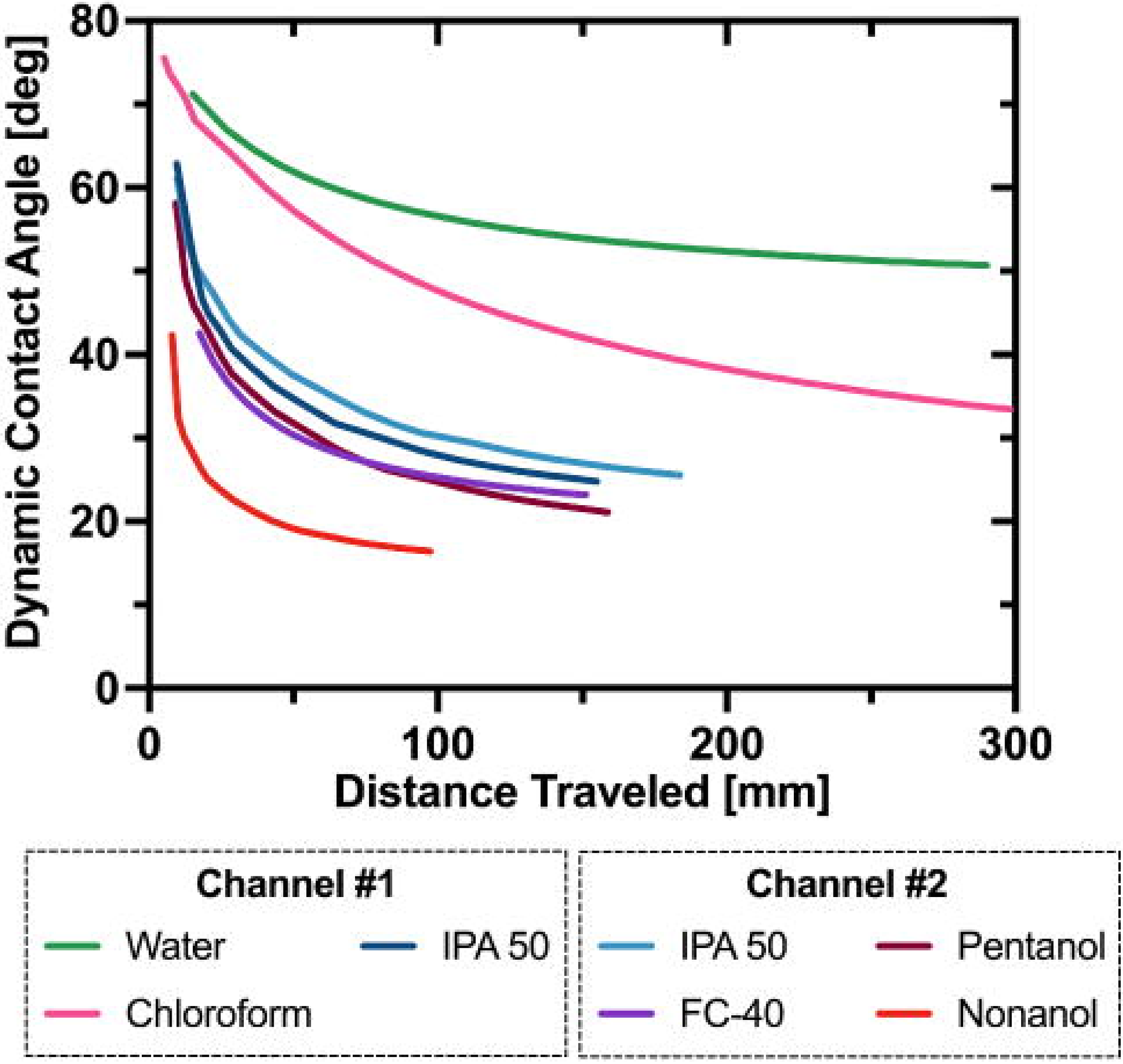
Dynamic Contact Angle [deg]
80
60
40
20
0
0
100
200
300
Distance Traveled [mm]
Channel #1
Water
IPA 50
Chloroform
Channel #2
IPA 50
Pentanol
FC-40
Nonanol

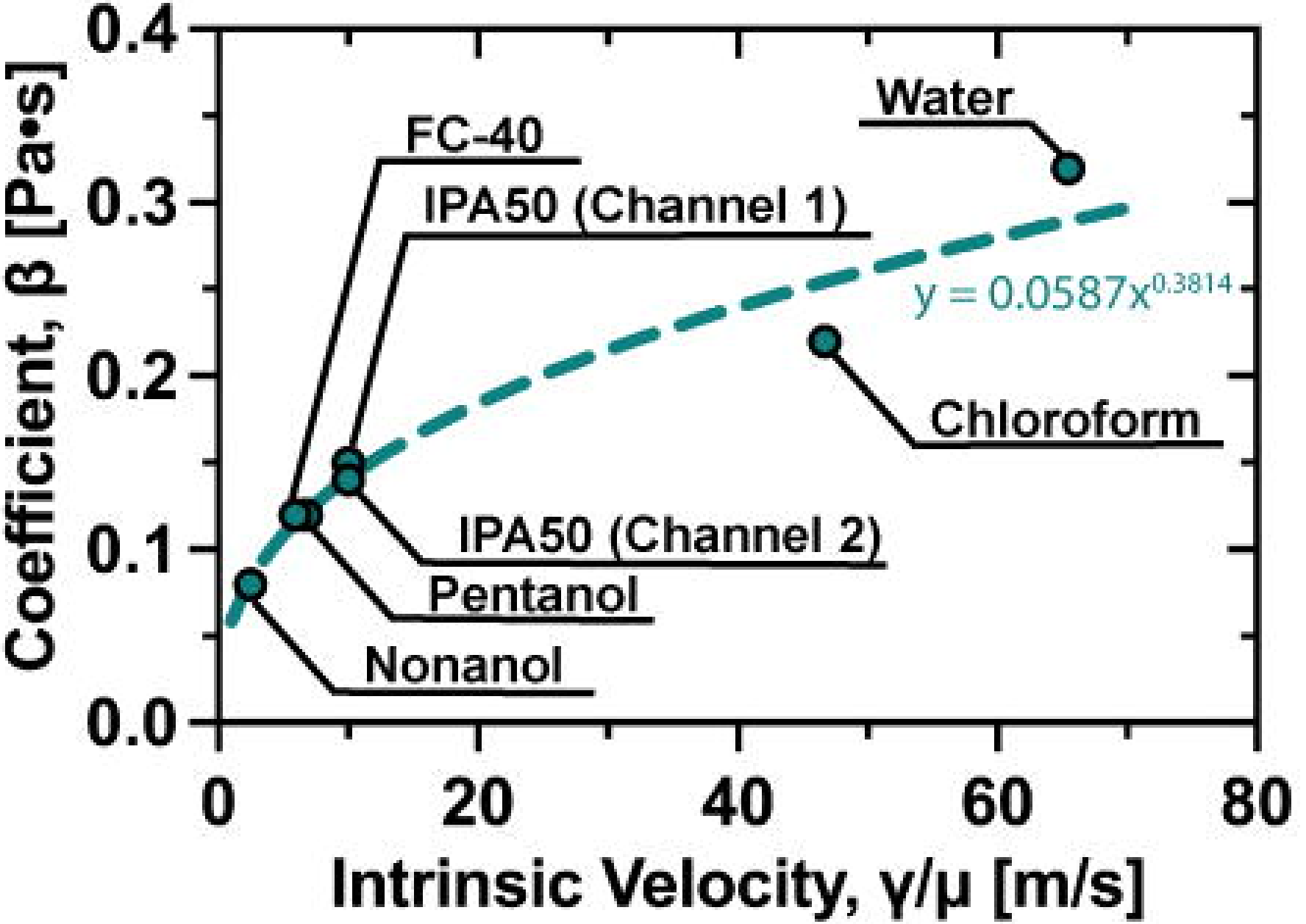
Coefficient, β [Pa•s]
0.4
0.3
0.2
0.1
0.0
0
20
40
60
80
Intrinsic Velocity, γ/μ [m/s]
Water
FC-40
IPA50 (Channel 1)
y = 0.0587x^0.3814
Chloroform
IPA50 (Channel 2)
Pentanol
Nonanol